

# Parametrizations of Inclusive Cross Sections for Pion Production in Proton-Proton Collisions

Steve R. Blattnig, Sudha R. Swaminathan, Adam T. Kruger,  
Moussa Ngom, and John W. Norbury

*Physics Department, University of Wisconsin - Milwaukee,  
P.O. Box 413, Milwaukee, Wisconsin 53201, USA.*

## Abstract

Accurate knowledge of cross sections for pion production in proton-proton collisions finds wide application in particle physics, astrophysics, cosmic ray physics and space radiation problems, especially in situations where an incident proton is transported through some medium, and one requires knowledge of the output particle spectrum given the input spectrum. In such cases accurate parametrizations of the cross sections are desired. In this paper we review much of the experimental data and compare to a wide variety of different cross section parametrizations. In so doing, we provide parametrizations of neutral and charged pion cross sections which provide a very accurate description of the experimental data. Lorentz invariant differential cross sections, spectral distributions and total cross section parametrizations are presented.

## 1. Introduction

Pion production in proton-proton collisions has been extensively studied over many years, and has now reached the point where this knowledge finds useful applications in a variety of areas, as detailed below.

1. Two important types of particle detectors are the hadronic and electromagnetic calorimeters [1], in which an electromagnetic or hadronic shower is initiated by a high energy incoming particle. From a Monte-Carlo simulation of the shower, one is able to deduce important characteristics of the incoming particle such as its energy and identity.

2. The primary cosmic rays can be detected by a variety of methods, depending on the incident energy. For the very high energy cosmic rays, where the flux is relatively low, the extensive air showers (EAS) [2, 3, 4] provide the most convenient means of detection. The EAS is analogous to the hadronic or electromagnetic calorimeter used in particle physics, but with the Earth's atmosphere being the active volume in which the shower develops. The EAS has both electromagnetic and hadronic components, and similar to the calorimeter, the energy and identity of primary cosmic ray nuclei can be deduced via Monte-Carlo simulation of the showers [2, 3].

3. In long duration human space flights, such as a mission to Mars, the radiation levels induced by galactic cosmic rays can exceed exposure limits set for astronauts [5, 6]. In determining the radiation environment inside a spacecraft one needs to transport the exterior cosmic ray spectrum through the spacecraft wall in order to determine the interior radiation spectrum.

4. In gamma ray [7, 8] and high energy neutrino astronomy [9, 10], the diffuse background radiation is due in large part to the gamma rays and neutrinos produced in proton collisions with the protons in the interstellar medium. In addition, pion production from proton-proton collisions finds applications in the calculation of gamma ray emission from the accretion disk around a black hole [11].

In all of the above applications it is crucial to have an accurate knowledge of the cross sections for pion production in proton-proton collisions. In addition, most of the applications mentioned above require solving the transport equations which determine the particle spectrum on one side of a material (active volume of calorimeter, Earth's atmosphere, spacecraft wall or interstellar medium) given the incident particle spectrum. Use of pion production cross sections in such transport codes requires that the cross section be written in a simple form. The transport codes have many iterative loops, which will take too much computer time if the cross section formulae also contain many iterative loops. Thus it is most advantageous if one can write down simple formulae which parameterize all of the experimental data on pion production cross sections. That is the aim of the present work.

In this paper we provide simple algebraic parametrizations of charged and neutral pion production cross sections valid over a range of energies. The cross sections we provide are Lorentz-invariant differential cross sections (LIDCS), lab frame spectral distributions (i.e.

energy differential cross sections) and total cross sections, because these are the types of cross sections most widely used in transport equations. Many authors have presented such parametrizations before, but the problem is to decide which authors are correct and whether a particular parametrization applies only to a limited data set or is valid over a wider range. In the present work, we have performed an exhaustive data search and have compared as many different parametrizations as possible to as much data as possible, so as to provide definitive conclusions as to which is the most accurate parametrization to use. All of this is discussed more extensively below.

The cross sections discussed in this paper are for inclusive pion production in proton-proton collisions, i.e. the reactions considered are  $p + p \rightarrow \pi + X$ , where  $p$  represents a proton,  $\pi$  represents a pion, and  $X$  represents any combination of particles. An extensive search for LIDCS data was performed, and the data was used to compare all available parametrizations. An extensive set of data was used in these comparisons, but only a few data points are graphed in this paper due to space considerations. A method for generating parametrizations for these cross sections is also described and applied to  $\pi^0$  production. Spectral distribution and total cross section formulae were not developed directly because of a lack of data. Instead, the most successful LIDCS parametrizations were first transformed into lab frame spectral distributions by numerical integration. These spectral distributions were parameterized and then numerically integrated to generate lab frame total cross sections. Finally, the total cross sections were compared to available data and parameterized as well. This procedure is discussed, and the parametrizations of the numerical results are given. Multiple checks of the accuracy of all results were made, and some of these are presented.

**Notation:** Starred quantities (e.g.  $\theta^*$ ) refer to the quantities in the center of mass (COM) frame, while unstarred quantities (e.g.  $\theta$ ) refer to the quantities in the lab frame.  $E \frac{d^3\sigma}{d^3p} \equiv$  Lorentz-Invariant Differential Cross Section (LIDCS)

$$\frac{d\sigma}{dE} \equiv \text{spectral distribution} = 2\pi p \int_0^{\theta_{max}} d\theta E \frac{d^3\sigma}{d^3p} \sin \theta$$

$$\sigma \equiv \text{total cross section} = 2\pi \int_0^{\theta_{max}} d\theta \int_{p_{min}}^{p_{max}} dp E \frac{d^3\sigma}{d^3p} \frac{p^2 \sin \theta}{\sqrt{p^2 + m_\pi^2}} = \int_{E_{min}}^{E_{max}} \frac{d\sigma}{dE} dE$$

$P_p$  is the proton momentum.

$m_p$  is the proton mass.

$m_\pi$  is the pion mass.

$\sqrt{s}$  is the magnitude of the total four momentum, and is equal to the total energy in the COM frame.

$T_{lab}$  is the lab frame kinetic energy of the incoming proton.

$T$  is the pion kinetic energy.

$E$  is the pion total energy.

$\theta$  is the angle of pion scattering with respect to the direction of the incident particle.

$p$  is the pion momentum.

$p_\perp \equiv p_t$  is the pion transverse momentum ( $p_\perp = p \sin \theta$ ).

$p_{max}$  is the maximum possible momentum the scattered pion can have for a given  $\sqrt{s}$ .

## 2. Comparison of Lorentz Invariant Differential Cross Sections

The object has been to determine an accurate parameterization for inclusive LIDCS, which can be confidently applied to regions where no experimental data is available. For example, the parametric equation would need to be extrapolated to energies lower than those for which data are available, if the formulae were to be used for the purpose of developing radiation shielding materials. The most convenient formulae are those that are in closed form, since they are easily used, and take relatively little CPU time in numerical calculations. Some of the formulae that were considered as representations of the LIDCS were not in closed form, but included tabulated functions of energy (i.e. numerical values were given for specific energy values rather than a functional form). When comparing parameterizations, closed form expressions were given precedence over other equally accurate formulae.

The invariant single-particle distribution is defined by

$$f(AB \rightarrow CX) \equiv E_c \frac{d^3\sigma}{d^3p_c} \equiv E \frac{d^3\sigma}{d^3p} = \frac{E}{p^2} \frac{d^3\sigma}{dpd\Omega} \quad (1)$$

where  $\frac{d^3\sigma}{d^3p_c}$  is the differential cross-section (i.e. the probability per unit incident flux) for detecting a particle  $C$  within the phase-space volume element  $d^3p_c$ .  $A$  and  $B$  are the initial colliding particles,  $C$  is the produced particle of interest, and  $X$  represents all other particles produced in the collision.  $E$  is the total energy of the produced particle  $C$ , and  $\Omega$  is the solid angle. This form is favored since the quantity is invariant under Lorentz transformations.

The data for pion production in proton-proton interactions is primarily reported in terms of the kinematic variables  $\theta^*$ ,  $\sqrt{s}$ ,  $p_\perp$ , which are respectively, the center of mass (COM) frame scattering angle of the pion, the invariant mass of the entire system, and the transverse momentum of the produced pion.  $\sqrt{s}$  is a Lorentz invariant quantity, and is equal to the total energy in the COM frame.  $p_\perp \equiv p^* \sin \theta^*$ , where  $p^*$  is the COM momentum.  $p_\perp$  is invariant under the transformation from the lab frame to the COM frame. (See [12] for a more detailed discussion of kinematic variables.) In the following discussions, all momenta, energies, and masses are in units of GeV.

### 2.1 Neutral Pions

Busser *et al.* [13] have fitted the LIDCS data obtained in the reaction  $p + p \rightarrow \pi^0 + X$ , where  $p$  represents a proton,  $\pi^0$  represents the neutral pion produced, and  $X$  represents all other produced particles, to an equation of the form

$$E \frac{d^3\sigma}{d^3p} = A p_\perp^{-n} \exp\left(-b \frac{p_\perp}{\sqrt{s}}\right) \quad (2)$$

with  $A = 1.54 \times 10^{-26}$ ,  $n = 8.24$ , and  $b = 26.1$ . This equation is based on a specific set of experimental data with all measurements taken at  $\theta^* \simeq 90^\circ$ , and was originally intended

only for pions with high  $p_{\perp}$ . Comparison of this parameterization with data available from other experiments [14] - [20] indicates that the global behavior of the invariant cross section cannot be represented by a function of this form. See Figures 1 - 3 for some examples of data. The parameterization of Busser *et al.* [13] was not plotted because the cross section is much too small compared to the data in the  $p_{\perp}$  ranges covered by the graphs.

The following form has been used by Albrecht *et al.* [21] to represent neutral pion production.

$$E \frac{d^3\sigma}{d^3p} = C \left( \frac{p_0}{p_{\perp} + p_0} \right)^n \quad (3)$$

where  $C$ ,  $n$ , and  $p_0$  are free parameters. This equation only has dependence on  $p_{\perp}$  where as the data [14] - [20], some of which is shown in Figures 1 - 3, also has dependence on  $\sqrt{s}$  and  $\theta^*$ . This form is therefore not general enough to represent all the data.

Ellis [22] have favored a representation for the invariant cross section of the form

$$E \frac{d^3\sigma}{d^3p} = A(p_{\perp}^2 + M^2)^{-N/2} f(x_{\perp}, \theta^*) \quad (4)$$

where  $f(x_{\perp}, \theta^*) = (1 - x_{\perp})^F$ ,  $N$  and  $F$  are free parameters and the scaling variable  $x_{\perp}$  is given by  $x_{\perp} = \frac{p_{\perp}}{p_{max}^*} \simeq \frac{2p_{\perp}}{\sqrt{s}}$ .  $p_{max}^* = [(s + m_{\pi}^2 - 4m_p^2)^2 / 4s - m_{\pi}^2]^{\frac{1}{2}}$ , where  $m_{\pi}$  and  $m_p$  are the mass of the neutral pion and the proton respectively, is the maximum pion momentum allowed. The outline of this basic form has been used by Carey *et al.* in fitting the invariant cross section for the inclusive reaction  $p + p \rightarrow \pi^0 + X$  [23]. Their representation is given by

$$E \frac{d^3\sigma}{d^3p} = A(p_{\perp}^2 + 0.86)^{-4.5} (1 - x_R^*)^4 \quad (5)$$

where  $x_R^* = \frac{p^*}{p_{max}^*}$  is the radial scaling variable and the normalization constant  $A$  has been determined as  $A \simeq 5$ . This parameterization accurately reproduces the data for measurements taken at  $\theta^* = 90^\circ$  and  $\sqrt{s} \geq 9.8$  GeV, but does not agree well with the data for lower energies ( $\sqrt{s} = 7$  GeV). The disagreement at lower energies can be seen in Figure 1.

Another problem with this parameterization becomes apparent, when one considers that integration over all allowed angles and outgoing particle momenta should yield the total inclusive cross section. The details of this calculation appear in Section 3. A comparison of the experimentally determined total cross section data from Whitmore [24] with the results of the numerical integration of equation [5] shows that the total cross section is greatly underestimated by Carey. See Figure 4.

Stephens and Badhwar [20] obtained data from the photon cross sections given by Fidecaro [14]. The Fidecaro data was taken at incident proton kinetic energy  $T_{lab} = 23$  GeV and  $p_{\perp} = 0.1$  GeV - 1.0 GeV. (Note: No error was listed by Fidecaro *et al.* [14] for pion production. Error bars of ten percent were added to the data on the figures, since this

level of error was standard for most of the other data. Also, Stephens uses the notation  $E_p$  instead of  $T_{lab}$ .) Figures 1 - 3, show common examples of the accuracy of Badhwar and Stephens' parameterization's fit to the data. The following is the parameterization of the  $\pi^0$  invariant cross section proposed by Stephens and Badhwar [20];

$$E \frac{d^3\sigma}{d^3p} = Af(T_{lab})(1 - \tilde{x})^q \exp(-Bp_{\perp}/(1 + 4m_p^2/s)) \quad (6)$$

where

$$\begin{aligned} \tilde{x} &= \sqrt{\{(x_{\parallel}^*)^2 + (\frac{4}{s})(p_{\perp}^2 + m_{\pi}^2)\}} \\ q &= \frac{C_1 - C_2 p_{\perp} + C_3 p_{\perp}^2}{\sqrt{1 + 4m_p^2/s}} \\ f(T_{lab}) &= (1 + 23T_{lab}^{-2.6})(1 - 4m_p^2/s)^2 \end{aligned}$$

and

$$A = 140, B = 5.43, C_1 = 6.1, C_2 = 3.3, C_3 = 0.6 \text{ with } x_{\parallel}^* \equiv \frac{p_{\parallel}^*}{p_{max}^*}, \text{ and } p_{\parallel}^* = p^* \cos \theta^*.$$

The Stephens-Badhwar parameterization was found to be the best of the previously listed representations, because it accurately reproduces the data in the low  $p_{\perp}$  region, where the cross section is greatest (see Figures 1 - 3), and its integration yields accurate values for the total cross section (see Figure 4). This equation is, however, a poor tool for predicting values of the invariant cross section for  $p_{\perp} \gtrsim 3$  GeV, where the value predicted underestimates experimental data by up to  $\simeq 10$  orders of magnitude (see Figures 2 and 3).

No parameterization currently exists that accurately fits the global behavior of the LIDCS data. Previous equations have suffered from being too specific to a particular set of experimental data, or from failing to reproduce the total cross section upon integration. It is for these reasons that a new parameterization is desired, one that correctly predicts all available data while maintaining the essential quality of correctly producing the total cross section upon integration.

The approach that has been adopted in the present work is to assume the following form for the invariant cross section

$$E \frac{d^3\sigma}{d^3p} = (\sin \theta^*)^{D(\sqrt{s}, p_{\perp}, \theta^*)} F(\sqrt{s}, p_{\perp}, \theta^* = 90^\circ) \quad (7)$$

The motivation for an equation of this form is that as the angle decreases, the cross section decreases very slowly at lower  $p_{\perp}$  values. The approximation that was made in deriving the above equation is that as  $p_{\perp} \rightarrow 0$ , the cross section is assumed to be independent of angle.

Under the assumption that the invariant cross section can be fitted by equation (7), the program goes as follows. Find a representation for the cross section as a function of energy  $\sqrt{s}$  and transverse momentum  $p_\perp$  from experimental data taken at  $\theta^* = 90^\circ$ .  $F(\sqrt{s}, p_\perp)$  is then completely determined, because  $(\sin \theta^*)^D$  is unity at  $\theta^* = 90^\circ$ .

At  $\theta^* = 90^\circ$  the data is well represented by

$$E \frac{d^3\sigma}{d^3p}(\theta^* = 90^\circ) \equiv F(\sqrt{s}, p_\perp),$$

with

$$F(\sqrt{s}, p_\perp) = \ln\left(\frac{\sqrt{s}}{\sqrt{s_{min}}}\right)G(q, p_\perp), \quad (8)$$

where  $q = s^{\frac{1}{4}}$  and the COM pion production threshold energy  $\sqrt{s_{min}} = 2m_p + m_\pi$ . The function,

$$G(q, p_\perp) \equiv \frac{E \frac{d^3\sigma}{d^3p}(\theta^* = 90^\circ)}{\ln\left(\frac{\sqrt{s}}{\sqrt{s_{min}}}\right)}$$

was parameterized as

$$G(q, p_\perp) = \exp\{k_1 + k_2 p_\perp + k_3 q^{-1} + k_4 p_\perp^2 + k_5 q^{-2} + k_6 p_\perp q^{-1} + k_7 p_\perp^3 + k_8 q^{-3} + k_9 p_\perp q^{-2} + k_{10} p_\perp^2 q^{-1} + k_{11} p_\perp^{-3}\} \quad (9)$$

with  $k_1 = 3.24$ ,  $k_2 = -6.046$ ,  $k_3 = 4.35$ ,  $k_4 = 0.883$ ,  $k_5 = -4.08$ ,  $k_6 = -3.05$ ,  $k_7 = -0.0347$ ,  $k_8 = 3.046$ ,  $k_9 = 4.098$ ,  $k_{10} = -1.152$ , and  $k_{11} = -0.0005$ . The parameters  $k_1 - k_{10}$  were obtained using the numerical curve fitting software Table Curve 3D v3 [26] and the eleventh term was added to modify the low  $p_\perp$  behavior of the parameterization.

With  $F(\sqrt{s}, p_\perp)$  determined, the function  $D(\sqrt{s}, p_\perp, \theta^*)$  is the only remaining unknown. Solving for  $D$  yields

$$D(\sqrt{s}, p_\perp, \theta^*) = \frac{\ln(E \frac{d^3\sigma}{d^3p}) - \ln(F(\sqrt{s}, p_\perp))}{\ln(\sin \theta^*)} \quad (10)$$

Equations (8) and (9) were then used in equation (10) to calculate values of  $D(\sqrt{s}, p_\perp, \theta^*)$ . If the function  $D$  is independent of angle, then equation (10) could be determined for any fixed angle,  $\theta^* \neq 90^\circ$ . Data were compared for a range of angular values, and this data revealed that the function  $D$  is not independent of angle. The angular dependence turned out to be of the form  $(\sin \theta^*)^{-0.45}$ , and

$$D(\sqrt{s}, p_\perp, \theta^*) = (\sin \theta^*)^{-0.45} [c_1 p_\perp^2 (\sqrt{s})^{c_3} + c_4 \frac{p_\perp}{\sqrt{s}} + \frac{c_5}{\sqrt{s}} + \frac{1.0}{s}] \quad (11)$$

with  $c_1 = 205.7$ ,  $c_2 = 3.308$ ,  $c_3 = -2.875$ ,  $c_4 = 10.43$ , and  $c_5 = 0.8$ .

*The final form of our resultant parameterization for the neutral pion invariant cross section in proton-proton collisions is equation (7) with  $F(p_\perp, \sqrt{s})$  given in equation (8),  $G(q, p_\perp)$  given in equation(9), and  $D(p_\perp, \sqrt{s}, \theta^*)$  given in equation(11). This form is accurate over a much greater range of transverse momentum values than those covered by previous representations. Figures 1 - 3 show a few comparisons. A much more extensive set of data was used in the development and comparison of the parameterizations, but they are not shown in this paper due to space considerations. For the low transverse momentum region where the cross section is the greatest, the fit is quite similar to that of Stephens *et al.* [20]. Also, Figure 4 shows that both formulae (6 and 7) integrate to approximately the same total cross section, which is in agreement with the data from Whitmore *et al.* [24]. (Equation 7 integrated into a total cross section is denoted as Kruger in Figure 4.) A more complete comparison of the integrated total cross section to data is given by Stephens *et al.* [20]. Note however that equation (7) was based mainly on the data from [14] - [20]. Equation (7) could therefore give unpredictable results in regions not included in those data sets, particularly for very low transverse momentum or  $\sqrt{s} \gg 63$  GeV.*



## 2.2 Charged Pions

The available data for charged pions, is less extensive than  $\pi^0$  data. There is therefore a higher degree of uncertainty in LIDCS for charged pions. Integration of a LIDCS to get a total cross section and comparison of the results to total cross section data, allows a check of the global fit of a parametrization. This check was made for charged as well as neutral pions, but due to a lack of data, it is more important for charged pions. Parametrizations that do not integrate to the correct total cross section can be ruled out, even if the LIDCS data is well represented, because the global behavior of the parametrization cannot be accurate. However, producing a correct total cross section upon integration does not necessarily imply that the global behavior of the parameterization is correct. A tighter constraint could be placed on possible LIDCS parametrizations, if more measurements were made. If the spectral distribution is measured at three different values of pion energy for two different proton collision energies, the general behavior of the spectral distribution could be checked. The angular dependence of LIDCS parametrization could then be tested by integrating over angle, and comparing the results to the spectral distribution data. For the purposes of space radiation shielding, measurements at proton lab kinetic energies of 3 GeV and 6 GeV, and pion lab kinetic energies of 0.01 GeV, 0.1 GeV, and 1 GeV would be useful, because this is the region with both a large cross section, and large Galactic Cosmic Ray fluxes. With these facts in mind, a comparison of LIDCS parametrizations with data from [16, 25, 27, 28, 29] for charged pion production follows.

A parametrization for  $\pi^-$  of the form

$$E \frac{d^3\sigma}{d^3p} = A \exp(-Bp_{\perp}^2) \quad (12)$$

has been given by Albrow *et al.* [29] where A and B are tabulated functions of  $x_R^* \equiv \frac{p^*}{p_{max}^*}$ . A and B are given only for  $x_R^* = 0.18$ ,  $x_R^* = 0.21$ , and  $x_R^* = 0.25$  which limits the usefulness of this parametrization.

Alper *et al.* [25] have fitted the data for both  $\pi^+$  and  $\pi^-$  production to the following form

$$E \frac{d^3\sigma}{d^3p} = A \exp(-Bp_{\perp} + Cp_{\perp}^2) \exp(-Dy^2) \quad (13)$$

where  $y$  is the longitudinal rapidity, and A, B, C, and D are tabulated functions of  $s$ , that are also dependent on the type of produced particle ( $\pi^+$  or  $\pi^-$ ). (Note that at  $\theta^* = 90^\circ$  we have  $y = 0$ .) The fit to the data is excellent for low transverse momentum, as can be seen in Figures 8 and 10, but these figures also show that this form has an increasing cross section for high  $p_{\perp}$ , which contradicts the trend in the data. Also, there are different sets of constants for each different energy, which makes a generalization to arbitrary energies difficult.

Parametrizations done by Carey *et al.* [30] and Ellis *et al.* [22] have a similar form, although Carey's was applied only to  $\pi^-$ . Both underestimate LIDCS for low  $p_{\perp}$ , where the cross section is the largest (see Figures 7-10).

The following is Carey's parametrization

$$E \frac{d^3\sigma}{d^3p}(\pi^-) = N(p_\perp^2 + 0.86)^{-4.5}(1 - x_R^*)^4 \quad (14)$$

where  $N=13$  is the overall normalization constant, and  $x_R^* \equiv \frac{p^*}{p_{max}^*} \approx \frac{2p^*}{\sqrt{s}}$ .

The following is Ellis's parametrization which was applied to both  $\pi^+$  and  $\pi^-$  production at  $\theta^* = 90^\circ$ .

$$E \frac{d^3\sigma}{d^3p} = A(p_\perp^2 + M^2)^{-N/2}(1 - x_\perp)^F \quad (15)$$

where  $M, N, F$  are given constants.  $A$  is an unspecified overall normalization for which we used  $A = 13$ , and  $x_\perp \equiv \frac{p_\perp}{p_{max}^*} \approx \frac{2p_\perp}{\sqrt{s}}$ .

The most successful LIDCS parametrization available for charged pion production was found to be the one developed by Badhwar *et al.* [31].

$$E \frac{d^3\sigma}{d^3p} = \frac{A(1 - \tilde{x})^q}{(1 + 4m_p^2/s)^r} e^{[-Bp_\perp/(1+4m_p^2/s)]} \quad (16)$$

where  $q$  is a function of  $p_\perp$  and  $s$ , such that

$$q = (C_1 + C_2 p_\perp + C_3 p_\perp^2)/(1 + 4m_p^2/s)^{1/2}$$

and

$$\tilde{x} \approx [x_\parallel^{*2} + \frac{4}{s}(p_\perp^2 + m_\pi^2)]^{1/2}$$

Here  $x_\parallel^* = \frac{p_\parallel^*}{p_{max}^*} \approx 2\frac{p_\parallel^*}{\sqrt{s}}$ . For  $\pi^+$ ,  $A = 153$ ,  $B = 5.55$ ,  $C_1 = 5.3667$ ,  $C_2 = -3.5$ ,  $C_3 = 0.8334$ , and  $r = 1$ . For  $\pi^-$ ,  $A = 127$ ,  $B = 5.3$ ,  $C_1 = 7.0334$ ,  $C_2 = -4.5$ ,  $C_3 = 1.667$ , and  $r = 3$ . This form is accurate for low transverse momentum (Figures 7-12), which is the most important region for radiation shielding due to the large cross section. It is also in closed form, so that extra numerical complexities do not have to be considered. A comparison to a few data points, shown in Figure 13, demonstrates that it integrates to the correct total cross section. A more detailed comparison of the integrated cross section to experimental data is given by Badhwar *et al.* [31]. Because of its relative accuracy and simplicity, this parametrization was integrated to get total cross sections and spectral distributions for charged pions.

Mokhov *et al.* [32] have also developed the following formulae for both  $\pi^+$  and  $\pi^-$  production.

$$E \frac{d^3\sigma}{d^3p} = A(1 - \frac{p^*}{p_{max}^*})^B \exp(-\frac{p^*}{C\sqrt{s}}) V_1(p_\perp) V_2(p_\perp) \quad (17)$$

where

$$\begin{aligned} V_1 &= (1 - D) \exp(-Ep_{\perp}^2) + D \exp(-Fp_{\perp}^2) \quad \text{for } p_{\perp} \leq 0.933 \text{ GeV} \\ &= \frac{0.2625}{(p_{\perp}^2 + 0.87)^4} \quad \text{for } p_{\perp} > 0.933 \text{ GeV} \end{aligned}$$

and

$$\begin{aligned} V_2 &= 0.7363 \exp(0.875p_{\perp}) \quad \text{for } p_{\perp} \leq 0.35 \text{ GeV} \\ &= 1 \quad \text{for } p_{\perp} > 0.35 \text{ GeV} \end{aligned}$$

with  $A=60.1$ ,  $B=1.9$ , and  $C=0.18$  for  $\pi^+$ ,  $A=51.2$ ,  $B=2.6$ , and  $C=0.17$  for  $\pi^-$ , and  $D=0.3$ ,  $E=12$ , and  $F=2.7$  for both  $\pi^+$  and  $\pi^-$ . Figures 7-12 show that the formula of Badhwar has a better fit to the data in the low  $p_{\perp}$  region where the cross section is the largest.

### 3. Spectral Distributions and Total Cross Sections

#### 3.1 Method of Generating Other Cross Sections from a LIDCS

While LIDCS contain all the necessary information for a particular process, sometimes other cross sections are needed. For example, one dimensional radiation transport requires probability density distributions that are integrated over solid angle. These quantities are calculated in terms of spectral distributions and total cross sections rather than LIDCS, but with accurate parametrizations of LIDCS, formulae for both spectral distributions and total cross sections can be developed. LIDCS for inclusive pion production in proton-proton collisions contain dependence on the energy of the colliding protons ( $\sqrt{s}$ ), on the energy of the produced pion ( $T_\pi$ ), and on the scattering angle of the pion ( $\theta$ ). Total cross sections  $\sigma$ , which depend only on  $\sqrt{s}$ , and spectral distributions  $\frac{d\sigma}{dE}$ , which depend on  $\sqrt{s}$  and  $T_\pi$  can be extracted from a LIDCS by integration. If azimuthal symmetry is assumed, these cross sections take the following forms

$$\frac{d\sigma}{dE} = 2\pi p \int_0^{\theta_{max}} d\theta E \frac{d^3\sigma}{d^3p} \sin\theta \quad (18)$$

$$\sigma = 2\pi \int_0^{\theta_{max}} d\theta \int_{p_{min}}^{p_{max}} dp E \frac{d^3\sigma}{d^3p} \frac{p^2 \sin\theta}{\sqrt{p^2 + m_\pi^2}} \quad (19)$$

where  $\theta_{max}$ ,  $p_{max}$ , and  $p_{min}$  are the extrema of the scattering angle and momentum of the pion respectively, and  $m_\pi$  is the rest mass of the pion.

In the Center of Mass (COM) frame these extrema can easily be determined. Using conservation of momentum and energy, one can easily show that

$$p^2 = \frac{(s + m_\pi^2 - s_x)^2}{4s} - m_\pi^2 \quad (20)$$

where  $s_x$  is the square of the invariant mass of the sum of all particles excluding the pion, and  $p$  is the magnitude of the three-momentum of the pion. The independence of  $p$  on  $\theta$  implies that  $\theta$  can take on all possible values (ie.  $\theta_{max} = \pi$ ), and the symmetry of the COM frame implies that  $p_{min} = 0$ . For a given value of  $s$ , it is obvious that momentum is a maximum when  $s_x$  is a minimum. An invariant mass is a minimum, when it is equal to the square of the sum of the rest masses of the particles in question. Momentum is, therefore, a maximum when  $s_x$  is the square of the sum of the least massive combination of particles that can be produced while still satisfying all relevant conservation laws. For the reaction  $p + p \rightarrow \pi + x$ , we have  $s_x \simeq 4m_p^2$ , where a subscript  $p$  represents a proton.

If a Lorentz transformation is applied to the maximum COM momentum, the integration limits can be determined in other frames. Byckling and Kajantie have shown that by transforming to the lab frame, the following formula can be obtained [12]

$$p_\pi^\pm = [p_a E_{max}^* \sqrt{s} \cos\theta \pm (E_a + m_p) \sqrt{sp_{max}^{*2} - m_\pi^2 p_a^2 \sin^2\theta}] [s + p_a^2 \sin^2(\theta)]^{-1} \quad (21)$$

where starred quantities are COM variables, and unstarred quantities are either lab or invariant variables,  $m_p$  is the rest mass of a proton;  $p_a$  is the magnitude of the momentum of the projectile proton, and  $p^+ = p_{max}$  is the maximum pion momentum. The greater of the two quantities  $p^- = p_{min}$  and 0 is the minimum pion momentum, and the maximum scattering angle can be determined by the requirement that  $p^\pm$  be real. This requirement implies that the quantity under the square root must be greater than or equal to 0. Solving for  $\theta_{max}$  then gives the formula

$$\theta_{max} = \sin^{-1}\left(\frac{\sqrt{s} p_{max}^*}{p_a m_\pi}\right) \quad (22)$$

With the limits of integration determined, a LIDCS can be turned into a total cross section or a spectral distribution by numerical integration. This procedure will, however, give discrete "data" points; not closed form expressions. Parametrizations of this numerical data are needed, if relatively simple formulae for these cross sections are desired. This process was completed for all three pion species, and the corresponding formulae are listed in the next section. It should be noted that the accuracy of these parametrizations is limited to that of the original LIDCS.

### 3.2 Parametrizations

The surface parametrizations for the spectral distribution as a function of incident proton kinetic energy in the lab frame ( $T_{lab}$ ) and the lab kinetic energy of the produced pion ( $T_\pi$ ) has been completed by numerically integrating LIDCS charged pion parametrizations due to Badhwar *et al.* (equation 16) [31] and the neutral pion cross section both from Stephens and Badhwar (equation 6) [20], and from equation 7. The numerical integration routines were checked by computing total cross sections in both the lab and COM frames and comparing the results. Since total cross section is invariant under the transformation between these two frames, the results should be the same in both frames. In order to accurately fit the integration points for low energies, it has been necessary to consider two regions of the surface and to determine representations for them individually. For each of the three pions, the two regions consist of laboratory kinetic energies ( $T_{lab}$ ) from 0.3 GeV to 2 GeV and from 2 GeV to 50 GeV. Using the following parametrizations in energy regions other than the region listed above could give unpredictable results since the formulae were not tested there.

The neutral pion spectral distribution for the range 0.3 - 2 GeV is represented by the following equations:

$$\begin{aligned}
F_2 &= A_1 T_\pi^{A_2} + A_3 T_{lab}^{A_4} \\
F_1 &= \exp\left(A_5 + \frac{A_6}{\sqrt{T_{lab}}}\right) + A_7 T_{lab}^{A_8} + A_9 T_\pi^{A_{10}} + A_{11} T_\pi^{A_{12}} \\
\left(\frac{d\sigma}{dE}\right)_{lab} &= \left(A_{13} \frac{F_1}{F_2} + A_{14} \exp\left(A_{16} \sqrt{T_\pi} + A_{17} T_\pi^{A_{18}} T_{lab}^{A_{19}}\right)\right) T_\pi^{A_{15}}
\end{aligned} \tag{23}$$

with constants  $A_i$  given in Table 1.

$A_1 = 6.78 \times 10^{-10}$	$A_8 = -1.75$	$A_{15} = 0.25$
$A_2 = -2.86$	$A_9 = -32.1$	$A_{16} = -39.4$
$A_3 = 1.82 \times 10^{-8}$	$A_{10} = 0.0938$	$A_{17} = 2.88$
$A_4 = -1.92$	$A_{11} = -23.7$	$A_{18} = 0.025$
$A_5 = 22.3$	$A_{12} = 0.0313$	$A_{19} = 0.75$
$A_6 = 0.226$	$A_{13} = 2.5 \times 10^6$	
$A_7 = -0.33$	$A_{14} = 1.38$	

Table 1: Constants for equation (23)

$B_1 = 1.3 \times 10^{-10}$	$B_8 = -1.25$	$B_{15} = 60322$
$B_2 = -2.86$	$B_9 = -33.2$	$B_{16} = 1.07$
$B_3 = 4.27 \times 10^{-9}$	$B_{10} = 0.0938$	$B_{17} = -67.5$
$B_4 = -2.4$	$B_{11} = -23.6$	
$B_5 = 22.3$	$B_{12} = 0.0313$	
$B_6 = -1.87$	$B_{13} = 2.5 \times 10^6$	
$B_7 = 1.28$	$B_{14} = 0.25$	

Table 2: Constants for equation (24)

The neutral pion spectral distribution for the range 2 - 50 GeV is represented by the following equations:

$$\begin{aligned}
F_2 &= B_1 T_\pi^{B_2} + B_3 T_{lab}^{B_4} \\
F_1 &= \exp\left(B_5 + \frac{B_6}{\sqrt{T_{lab}}}\right) + B_7 T_{lab}^{B_8} + B_9 T_\pi^{B_{10}} + B_{11} T_\pi^{B_{12}} \\
\left(\frac{d\sigma}{dE}\right)_{lab} &= B_{13} T_\pi^{B_{14}} \frac{F_1}{F_2} + B_{15} T_\pi^{B_{16}} \exp\left(B_{17} \sqrt{T_\pi}\right)
\end{aligned} \tag{24}$$

with constants  $B_i$  given in Table 2.

The positively charged pion spectral distribution for the range 0.3 - 2 GeV is represented by the following equations:

$$\begin{aligned}
F_2 &= C_1 T_\pi^{C_2} + C_3 T_{lab}^{C_4} \\
F_1 &= \exp\left(C_5 + \frac{C_6}{\sqrt{T_{lab}}}\right) + C_7 T_{lab}^{C_8} + C_9 T_\pi^{C_{10}} + C_{11} T_\pi^{C_{12}} T_{lab}^{C_{13}} + C_{14} \ln T_{lab} \\
\left(\frac{d\sigma}{dE}\right)_{lab} &= C_{15} T_\pi^{C_{16}} \frac{F_1}{F_2} + C_{17} T_\pi^{C_{18}} \exp(C_{19} \sqrt{T_\pi} + C_{20} \sqrt{T_{lab}})
\end{aligned} \tag{25}$$

with constants  $C_i$  given in Table 3.

$C_1 = 2.2 \times 10^{-8}$	$C_8 = -1.75$	$C_{15} = 2.5 \times 10^6$
$C_2 = -2.7$	$C_9 = -29.4$	$C_{16} = 0.25$
$C_3 = 4.22 \times 10^{-7}$	$C_{10} = 0.0938$	$C_{17} = 976$
$C_4 = -1.88$	$C_{11} = -24.4$	$C_{18} = 2.3$
$C_5 = 22.3$	$C_{12} = 0.0312$	$C_{19} = -46$
$C_6 = 1.98$	$C_{13} = 0.0389$	$C_{20} = -0.989$
$C_7 = -0.28$	$C_{14} = 1.78$	

Table 3: Constants for equation (25)

$D_1 = 4.5 \times 10^{-11}$	$D_7 = -35.3$	$D_{13} = 60322$
$D_2 = -2.98$	$D_8 = 0.0938$	$D_{14} = 1.18$
$D_3 = 1.18 \times 10^{-9}$	$D_9 = -22.5$	$D_{15} = -72.2$
$D_4 = -2.55$	$D_{10} = 0.0313$	$D_{16} = 0.941$
$D_5 = 22.3$	$D_{11} = 2.5 \times 10^6$	$D_{17} = 0.1$
$D_6 = -0.765$	$D_{12} = 0.25$	

Table 4: Constants for equation (26)

The positively charged pion spectral distribution for the range 2 - 50 GeV is represented by the following equations:

$$\begin{aligned}
F_2 &= D_1 T_\pi^{D_2} + D_3 T_{lab}^{D_4} \\
F_1 &= \exp\left(D_5 + \frac{D_6}{\sqrt{T_{lab}}}\right) + D_7 T_\pi^{D_8} + D_9 T_\pi^{D_{10}} \\
\left(\frac{d\sigma}{dE}\right)_{lab} &= D_{11} T_\pi^{D_{12}} \frac{F_1}{F_2} + D_{13} T_\pi^{D_{14}} \exp(D_{15} \sqrt{T_\pi} + D_{16} T_{lab}^{D_{17}})
\end{aligned} \tag{26}$$

with constants  $D_i$  given in Table 4.

The negatively charged pion spectral distribution for the range 0.3 - 2 GeV is represented by the following equations:

$$\begin{aligned}
F_2 &= G_1 T_\pi^{G_2} + G_3 T_{lab}^{G_4} \\
F_1 &= \exp\left(G_5 + \frac{G_6}{\sqrt{T_{lab}}}\right) + G_7 T_\pi^{G_8} + G_9 T_\pi^{G_{10}} \\
\left(\frac{d\sigma}{dE}\right)_{lab} &= T_\pi^{G_{11}} \left(G_{12} \frac{F_1}{F_2} + G_{13} \exp(G_{14} \sqrt{T_\pi})\right)
\end{aligned} \tag{27}$$

with constants  $G_i$  given in Table 5.

$G_1 = 1.06 \times 10^{-9}$	$G_6 = -1.5$	$G_{11} = 0.25$
$G_2 = -2.8$	$G_7 = -30.5$	$G_{12} = 2.5 \times 10^6$
$G_3 = 3.7 \times 10^{-8}$	$G_8 = 0.0938$	$G_{13} = 7.96$
$G_4 = -1.89$	$G_9 = -24.6$	$G_{14} = -49.5$
$G_5 = 22.3$	$G_{10} = 0.0313$	

Table 5: Constants for equation (27)

$H_1 = 2.39 \times 10^{-10}$	$H_7 = -31.3$	$H_{13} = 60322$
$H_2 = -2.8$	$H_8 = 0.0938$	$H_{14} = 1.1$
$H_3 = 1.14 \times 10^{-8}$	$H_9 = -24.9$	$H_{15} = -65.9$
$H_4 = -2.3$	$H_{10} = 0.0313$	$H_{16} = -9.39$
$H_5 = 22.3$	$H_{11} = 2.5 \times 10^6$	$H_{17} = -1.25$
$H_6 = -2.23$	$H_{12} = 0.25$	

Table 6: Constants for equation (28)

The negatively charged pion spectral distribution for the range 2 - 50 GeV is represented by the following equations:

$$\begin{aligned}
F_2 &= H_1 T_\pi^{H_2} + H_3 T_{lab}^{H_4} \\
F_1 &= \exp(H_5 + \frac{H_6}{\sqrt{T_{lab}}} + H_7 T_\pi^{H_8} + H_9 T_\pi^{H_{10}}) \\
(\frac{d\sigma}{dE})_{lab} &= H_{11} T_\pi^{H_{12}} \frac{F_1}{F_2} + H_{13} T_\pi^{H_{14}} \exp(H_{15} \sqrt{T_\pi} + H_{16} T_{lab}^{H_{17}})
\end{aligned} \tag{28}$$

with constants  $H_i$  given in Table 6.

Total inclusive cross sections are represented by the following equations.

$$\sigma_{\pi^0} = (0.007 + 0.1 \frac{\ln(T_{lab})}{T_{lab}} + \frac{0.3}{T_{lab}^2})^{-1} \tag{29}$$

$$\sigma_{\pi^+} = (0.00717 + 0.0652 \frac{\ln(T_{lab})}{T_{lab}} + \frac{0.162}{T_{lab}^2})^{-1} \tag{30}$$

$$\sigma_{\pi^-} = (0.00456 + \frac{0.0846}{T_{lab}^{0.5}} + \frac{0.577}{T_{lab}^{1.5}})^{-1} \tag{31}$$

For neutral pions, spectral distributions and total cross sections that were based on our own parametrization given in equation (7) were also developed. The formula for the spectral distribution was not divided into two regions, and it is much simpler than the previous formulae.

$$(\frac{d\sigma}{dE})_{lab} = \exp(K_1 + \frac{K_2}{T_{lab}^{0.4}} + \frac{K_3}{T_\pi^{0.2}} + \frac{K_4}{T_\pi^{0.4}}) \tag{32}$$

where  $K_1 = -5.8$ ,  $K_2 = -1.82$ ,  $K_3 = 13.5$ ,  $K_4 = -4.5$ .

Because equation (7) and Stephens LIDCS parametrization integrate to nearly the same total cross section (see Figure 4), separate total cross section parametrizations are not necessary (i.e. use equation 29).

### 3.3 Discussion of Figures

As discussed previously, Figures 1 - 3 show a comparison of LIDCS parametrizations for  $\pi^0$  production of Carey *et al.* (equation 5) [15], Stephens *et al.* (equation 6) [20], and



equation (7) plotted with data from [14] - [20]. The figures are graphs of cross section plotted against transverse momentum ( $p_{\perp}$ ) for various values of COM energy ( $E_{cm}$ ) and COM scattering angle ( $\theta^*$ ). Figure 1 shows that the parametrization of Carey *et al.* is not an adequate representation of the data. Figures 2 and 3 show that the parametrization of Stephens *et al.* fails for high transverse momentum by severely underpredicting the cross section.

Figure 4 shows numerically integrated LIDCS parametrizations of Stephens *et al.* (equation 6) [20], of Carey *et al.* (equation 5) [15], and of equation (7) (referred to as Kruger) for  $\pi^0$  production plotted with a parametrization of the integrated formulae of Stephens *et al.* referred to as Stephens-total-param (equation 29). Three data points from Whitmore [24] show that Carey's parametrization does not integrate to the correct values and that the rest are quite accurate (see [20] for more detail).

Figure 5 shows  $\pi^0$  spectral distribution parametrizations given by equations (23) and (24) plotted with LIDCS parametrization of Stephens (equation 6) numerically integrated at several lab kinetic energies. Figure 6 shows  $\pi^0$  spectral distribution parametrizations given by equation (32) plotted with the numerical integration of equation (7). The shapes of the two spectral distributions look quite different even though both original LIDCS formula have a similar fit to the data at low  $p_{\perp}$  where the cross section is the greatest, and both integrate to the same total cross section. This implies that the available data is not sufficient to tightly constrain the shape of the spectral distribution.

As discussed previously, Figures 7 - 12 show  $\pi^+$  and  $\pi^-$  LIDCS parametrizations of Alper *et al.* (equation 13) [25], Badhwar *et al.* (equation 16) [31], Ellis *et al.* (equation 15) [22], Carey *et al.* (equation 14) [30], and Mokhov *et al.* (equation 17) [32] and LIDCS data from [16, 25] plotted against transverse momentum ( $p_t \equiv p_{\perp}$ ) for different values of COM energy ( $E_{cm}$ ), but all at  $\theta^* = 90^\circ$ . These graphs show that the parametrizations of Badhwar best fit the data, but underpredict the cross section for large transverse momentum.

Figure 13 shows the numerically integrated LIDCS parametrizations of Badhwar *et al.* (equation 16) [31], and of Carey *et al.* (equation 14) [30] for  $\pi^+$  and  $\pi^-$  plotted with parametrizations of the integrated formulae of Badhwar referred to as present work (equations 30 and 31). Three data points from Whitmore *et al.* [24] show that Carey's parametrization does not integrate to the correct values and that Badhwar's formula is accurate. The figures also show that the parametrization fits the numerically integrated formulae very well.

Figures 14 and 15 show  $\pi^-$  and  $\pi^+$  spectral distribution parametrizations plotted with LIDCS parametrization of Badhwar *et al.* (equation 16) [31] numerically integrated. The plot is of cross section ( $\frac{d\sigma}{dE}$ ) plotted against the kinetic energy of the produced pion  $T_{\pi}$  at several values for the lab kinetic energies of the colliding proton. The graphs clearly show that the spectral distribution parametrizations have excellent fits to the integrated LIDCS parametrizations.

## 4. Summary and Conclusions

This paper presents parametrizations of cross sections for inclusive pion production in proton-proton collisions. The cross sections of interest are Lorentz Invariant Differential Cross Sections (LIDCS), lab frame spectral distributions, and total cross sections. For neutral pions the parametrization of Stephens *et al.* [20] (equation 6) fit the data well for low values of  $p_{\perp}$ , but overpredicted the cross section by many orders of magnitude at high  $p_{\perp}$  values. Because of this inaccuracy, equation (7) was developed. *The final form of our resultant parametrization for the neutral pion invariant cross section in proton-proton collisions is equation (7) with  $D(p_{\perp}, \sqrt{s}, \theta^*)$  given in equation (11),  $F(p_{\perp}, \sqrt{s})$  given in equation (8), and  $G(q, p_{\perp})$  given in equation(9).* This formula is as accurate as that of Stephens *et al.* [20] at low  $p_{\perp}$  values, but is much more accurate at high  $p_{\perp}$  values. For charged pions the formulae of Badhwar *et al.* (equation 16) [31] were found to best represent the data except at high  $p_{\perp}$  values. These formulae were used in the development of spectral distributions and total cross sections because they are the most accurate at low  $p_{\perp}$  where the cross section is the greatest.

The data for lab frame spectral distributions and total cross sections is scarce, so parametrizations for these quantities were developed using the above LIDCS formulae. These formulae were numerically integrated, resulting in discrete numerical "data" points for these other cross sections. The accuracy of the representations of lab frame spectral distributions and total cross sections is, therefore, limited to the accuracy of the original LIDCS. The numerical "data" was then parametrized so that closed form expressions (equations 23-32) could be obtained. As a check on the accuracy, the total cross section numerical "data" was compared to experimental data. They were found to agree quite well, but when the numerical "data" for the spectral distributions for the formulae for  $\pi^0$  production (equations 23-24 and 32) are compared (ie. compare Figure 5 to Figure 6), they are found to disagree. Since both original LIDCS formulae fit the data well at low  $p_{\perp}$  where the cross section is greatest, and both formulae integrate to the correct total cross section, the available data must not be sufficient to uniquely determine the global behavior of the LIDCS. The data for charged pion production is much more limited than the data for neutral pion production, so the same problem exists for charged pions.

To more accurately determine the cross sections for space radiation applications, measurements of the spectral distribution at lower energies (for example, proton lab kinetic energies 3 and 8 GeV, and pion lab kinetic energies of 0.01 GeV, 0.1 GeV, and 1 GeV) would need to be taken. These measurements would put a much tighter constraint on the global properties of the LIDCS, and the spectral distribution parametrizations could also be made more accurate.

### Acknowledgements:

The authors would like to thank Sean Ahern, and Alfred Tang for their help on the project. SRB was supported by the Wisconsin Space Grant Consortium, NASA grant

NCC-1-260, and NASA Graduate Student Researchers Program Fellowship NGT-52217. ATK and MN were supported by the Wisconsin Space Grant Consortium, NASA grant NCC-1-260, and NSF grant PHY-9507740. JWN and SRS were supported by NASA grants NCC-1-260, and NCC-1-354.

## Appendix A. Synopsis of Data Transformations

The data that was used in the comparison of different parametrizations was given in terms of several different kinematic variables. Some of the LIDCS data was transformed so that all data would be expressed in terms of the same variables:  $p_{\perp}$ ,  $\theta^*$ , and  $E_{cm} = \sqrt{s}$ . The following is a synopsis of the transformations that were performed for the data plotted in the figures.

The data from Carey *et al.* [15] was listed for different values of  $P_p$ ,  $p_{\perp}$ , and  $\theta$ .  $\sqrt{s}$ ,  $p_{\perp}$ , and  $\theta$  were used by Eggert *et al.* Stephens *et al.* [20] used photon production data from Fidecaro *et al.* [14] to derive pion production cross sections. The variables  $T_{lab}$ ,  $\theta$ , and  $p$  were used by Stephens.  $\sqrt{s}$ ,  $p_{\perp}$ , and the longitudinal rapidity  $y$  were used by Alper *et al.* [25], but only data with  $y = 0$  was used in the figures. When  $y = 0$  then  $\theta^* = 90^\circ$ .

The necessary transformations are as follows.

$$p_{\perp} = p \sin \theta \quad (33)$$

$T_{lab}$ ,  $P_p$ , and  $\theta$  can be transformed into  $\sqrt{s}$  and  $\theta^*$  by using the following Lorentz transformations to change to the COM frame. First express  $T_{lab}$  and  $P_p$  as total lab energy  $E$ .

$$E = T_{lab} + m_p = \sqrt{P_p^2 + m_p^2} \quad (34)$$

Now perform the following Lorentz transformations.

$$E_{cm} = -\gamma v p \cos \theta + \gamma E \quad (35)$$

$$\theta^* = \tan^{-1}\left(\frac{p \sin \theta}{\gamma p \cos \theta - \gamma v E}\right) \quad (36)$$

where

$$\gamma = \frac{T_{lab} + 2m_p}{\sqrt{s}} \quad (37)$$

$$v = \sqrt{1 - \gamma^{-2}} \quad (38)$$

## References

- [1] R. Fernow, Introduction to experimental particle physics (Cambridge University Press, New York, 1986); K. Kleinknecht, Detectors for Particle Radiation, 2nd ed., (Cambridge University Press, New York, 1998).
- [2] M.V.S. Rao and B.V. Sreekantan, Extensive Air Showers (World Scientific, Singapore, 1998).
- [3] T.K. Gaisser, Cosmic Rays and Particle Physics (Cambridge University Press, New York, 1990).
- [4] P. Sokolsky, Introduction to Ultrahigh energy cosmic ray physics (Addison-Wesley, Redwood City, California, 1989).
- [5] J.W. Wilson *et al.*, Transport Methods and Interactions for Space Radiations, NASA Reference Publication, No.1257, (1991).
- [6] J.L. Shinn *et al.*, IEEE Trans. Nucl. Sc., 45, pp. 2711 - 2719 (1998).
- [7] M.S. Longair, High energy astrophysics, vol. 2, 2nd ed., (Cambridge University Press, New York, 1992).
- [8] C.D. Dermer, Astrophysical J., 307, pp. 47 - 59 (1986); Astron. Astrophys., 157, pp. 223 - 229 (1986).
- [9] F.W. Stecker, C. Done, M.H. Salmon and P. Sommers, Phys. Rev. Lett., 66, pp. 2697 - 2700 (1991); *ibid.* vol. 69, pp. 2738 (1992).
- [10] R.J. Protheroe, Nucl. Phys. B Supplement, 43, pp. 229 - 236 (1995).
- [11] R. Mahadevan, R. Narayan and J. Krolik, Astrophysical J., 486, pp. 268-275 (1997).
- [12] E. Byckling and K. Kajantie, *Particle Kinematics*, John Wiley & Sons (1973)
- [13] F. W. Busser *et al.*, Phys. Lett. B 46, pp. 471-476 (1973)
- [14] M. Fidecaro *et al.*, Nuovo Cimento 24, pp. 73-86 (1962)
- [15] D. C. Carey *et al.*, Phys. Rev. D 14, pp. 1196-1216 (1976)
- [16] F. W. Busser *et al.*, Nucl. Phys. B 106, pp. 1-30 (1976)
- [17] K. Eggert *et al.*, Nucl. Phys. B 98, pp. 49-72. (1975)

- [18] D. Lloyd Owen *et al.*, Phys. Rev. Lett. 45, pp. 89 (1980) The complete set of data is not given in the paper, but is listed at <http://durpdg.dur.ac.uk/scripts/tabkum.csh/TABLE/3770/999/1/1>.
- [19] A. L. S. Angelis *et al.*, Phys. Lett. B 185, pp. 213-217 (1987)
- [20] S. A. Stephens and G. D. Badhwar, Astrophysics and Space Science 76, pp. 213-233 (1981)
- [21] R. Albrecht *et al.*, Eur. Phys. J. C 5 pp.255-267 (1998)
- [22] S. D. Ellis and R. Stroynowski, Rev. of Mod. Phys. 49, pp. 753-775 (1977)
- [23] D. C. Carey *et al.*, Phys. Rev. Lett. 33, pp. 327-330. (1974)
- [24] J. Whitmore, Phys Reports C, 10, pp. 273-373 (1974)
- [25] B. Alper *et al.*, Nucl. Phys. B 100, pp. 237-290 (1975)
- [26] Manufactured by SPSS Inc., Table Curve 3D v3, Copyright 1997 by AISN Software Inc.
- [27] P. Capiluppi *et al.*, Nucl. Phys. B 79, pp. 189-258 (1974)
- [28] P. Capiluppi, G. Giacomelli, A. M. Rossi, G. Vannini, A. Bussiere, Nucl. Phys. B 70, pp. 1-38 (1974)
- [29] M. G. Albrow *et al.*, Phys. Lett. B 42, pp. 279-282 (1972)
- [30] D. C. Carey *et al.*, Phys. Rev. Lett. 33, pp 330-333 (1974)
- [31] G. D. Badhwar, S. A. Stephens, R. L. Golden, Phys. Rev. D 15, pp. 820-831 (1977)
- [32] N. V. Mokhov and S. I. Striganov, CP435, *Workshop on the Front End of a Muon Collider*, pp. 453-459 (1998).

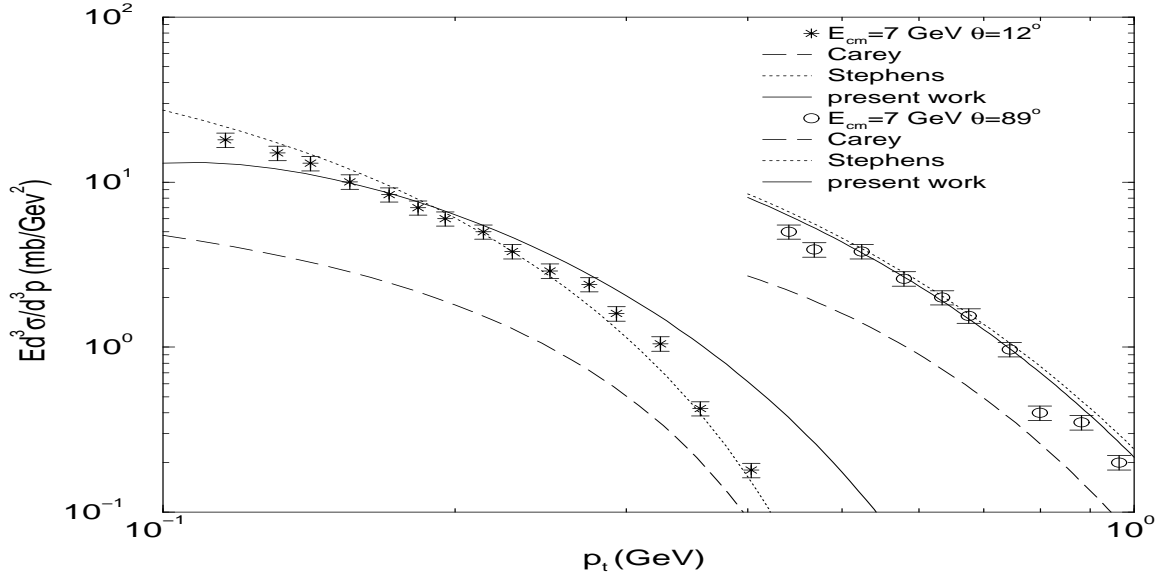


Figure 1:  $\pi^0$  production parametrizations of Carey et al. (equation 5) [15], of Stephens et al. (equation 6) [20], and of equation (7) plotted with LIDCS data from [14, 20]. LIDCS is plotted against transverse momentum for COM energy  $E_{cm} = 7 \text{ GeV}$ . The pion COM scattering angle is  $12.2 < \theta^* < 12.4^\circ$  and  $\theta^* = 89^\circ$  for the data, and the parametrizations are plotted at  $\theta^* = 12^\circ$  and  $\theta^* = 89^\circ$ .

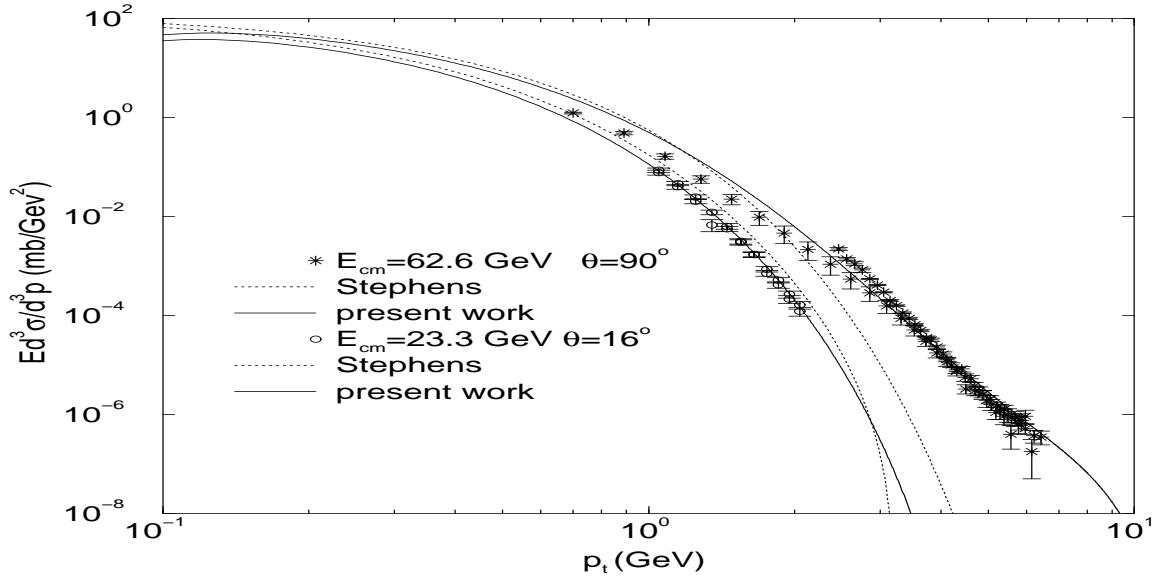


Figure 2:  $\pi^0$  production parametrizations of Carey et al. (equation 5) [15], of Stephens et al. (equation 6) [20], and of equation (7) plotted with LIDCS data from [13, 16, 17]. The data is for COM energy  $E_{cm} = 62.4$  GeV and 62.9 GeV at COM scattering angle  $\theta^* = 90^\circ$  and the parametrizations are plotted at  $E_{cm} = 62.6$  GeV at  $\theta^* = 90^\circ$ . The second set of data is at COM energy  $E_{cm} = 23.3$  GeV and the pion COM scattering angle  $\theta^* = 15^\circ$  and  $17.5^\circ$  for the data, and the parametrizations are plotted at  $\theta^* = 16^\circ$ .



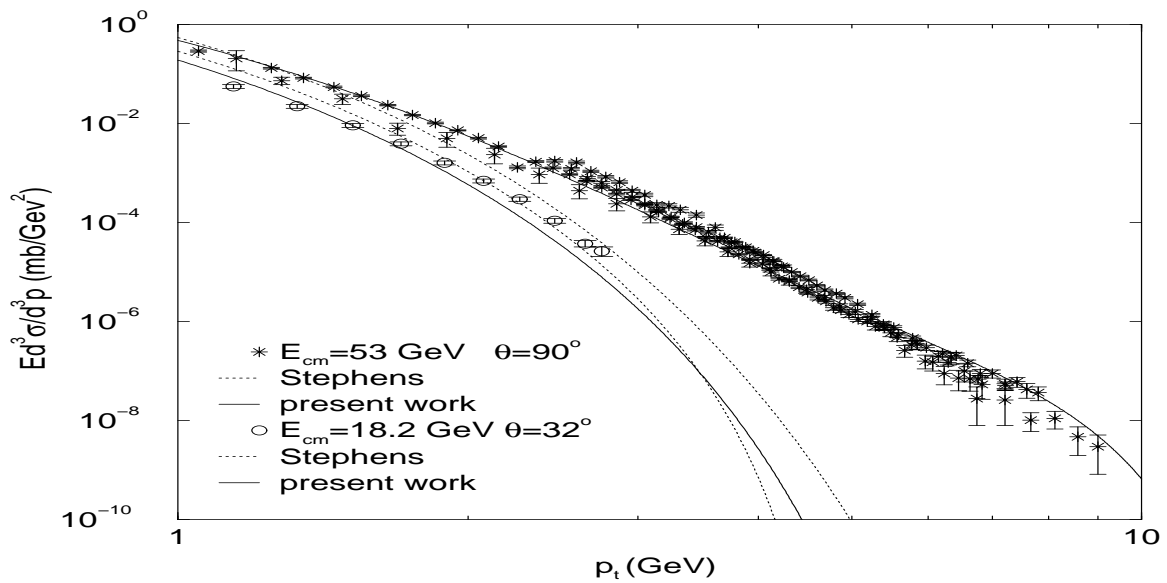


Figure 3:  $\pi^0$  production parametrizations of Carey et al. (equation 5) [15], of Stephens et al. (equation 6) [20], and of equation (7) plotted with LIDCS data from [15]. LIDCS is plotted against transverse momentum for COM energy  $E_{cm} = 18.2$  GeV. The pion COM scattering angle  $32.3^\circ < \theta^* < 32.5^\circ$  for the data, and the parametrizations are plotted at  $\theta^* = 32^\circ$ . The second set of data and parametrizations are at  $E_{cm} = 53$  GeV,  $\theta^* = 90^\circ$ . The data is from [13, 16, 17, 18].

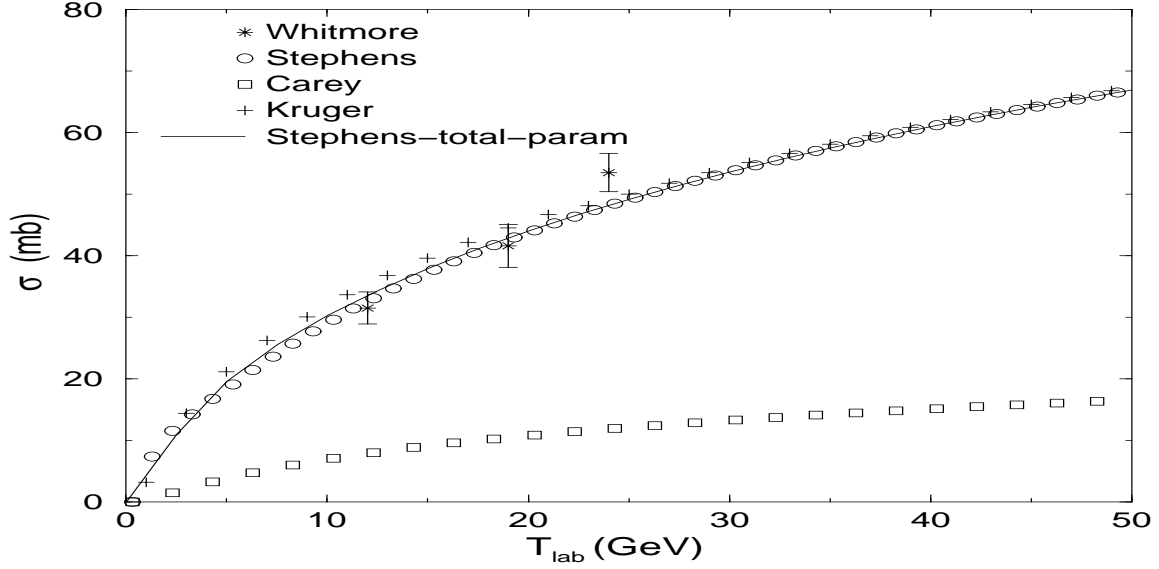


Figure 4: Parametrization of total  $\pi^0$  production cross section plotted with *numerically integrated* LIDCS parametrizations of Stephens et al. (equation 6) [20], of Carey et al. (equation 5) [15], and of equation(7) referred to as Kruger. The curve labelled ‘Stephens-total-param’ is the parametrization given in equation (29). Three data points from Whitmore [24] are included for comparison.

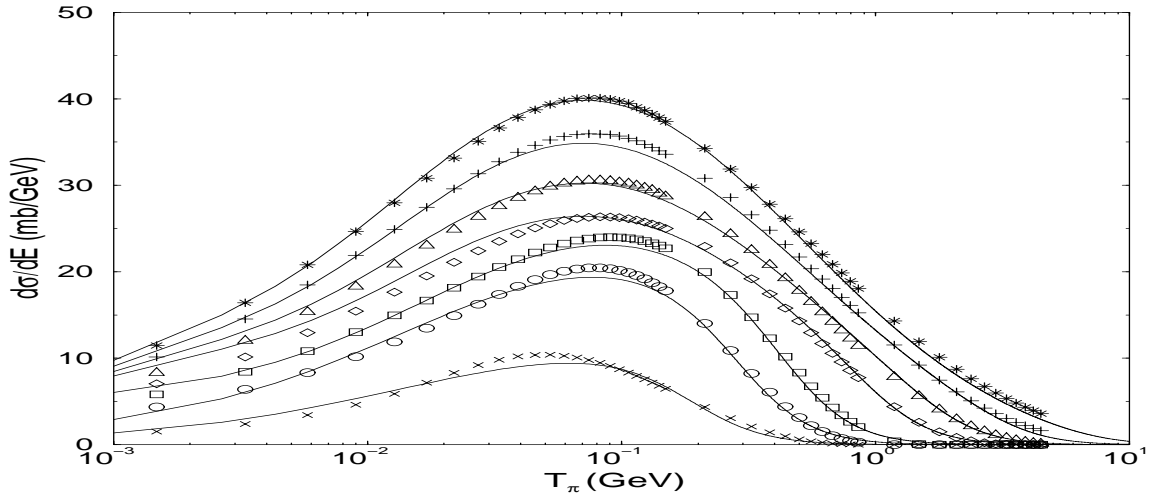


Figure 5:  $\pi^0$  spectral distribution parametrizations of equations (23) and (24) (solid lines) plotted with LIDCS parametrization of Stephens (equation 6) [20] numerically integrated at lab kinetic energies of 0.5 GeV, 1.0 GeV, 1.9 GeV, 5.0 GeV, 9.5 GeV, 20 GeV, and 50 GeV, listed in order of increasing cross section (symbols).

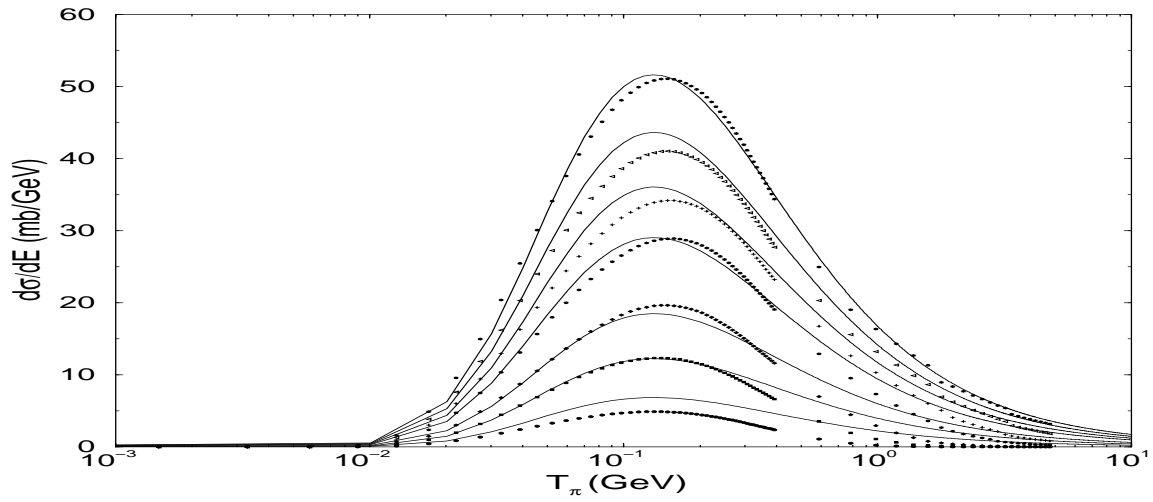


Figure 6:  $\pi^0$  spectral distribution parametrization of equation (32) (solid lines) plotted with equation(7) numerically integrated at lab kinetic energies of 0.5 GeV, 1.0 GeV, 1.9 GeV, 5.0 GeV, 9.5 GeV, 20 GeV, and 50 GeV, listed in order of increasing cross section (symbols).

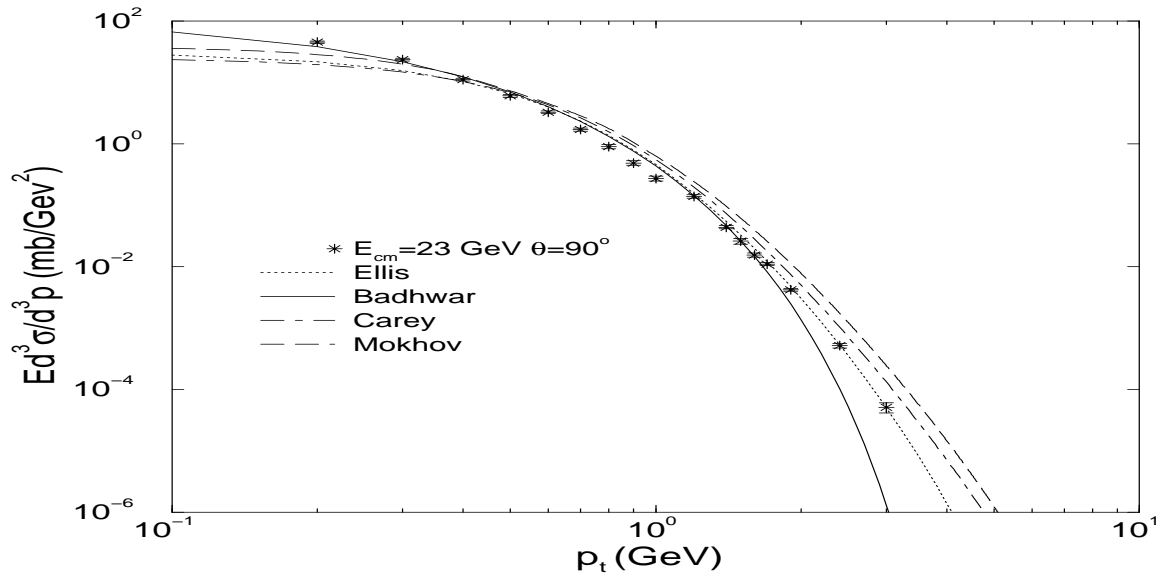


Figure 7:  $\pi^-$  production parametrizations of Ellis *et al.* (equation 15) [22], Badhwar *et al.* (equation 16) [31], Carey *et al.* (equation 14) [30], and of Mokhov *et al.* (equation 17) [32] plotted with LIDCS data from [25]. LIDCS is plotted against transverse momentum for COM energy  $E_{cm} = 23$  GeV and pion COM scattering angle  $\theta^* = 90^\circ$

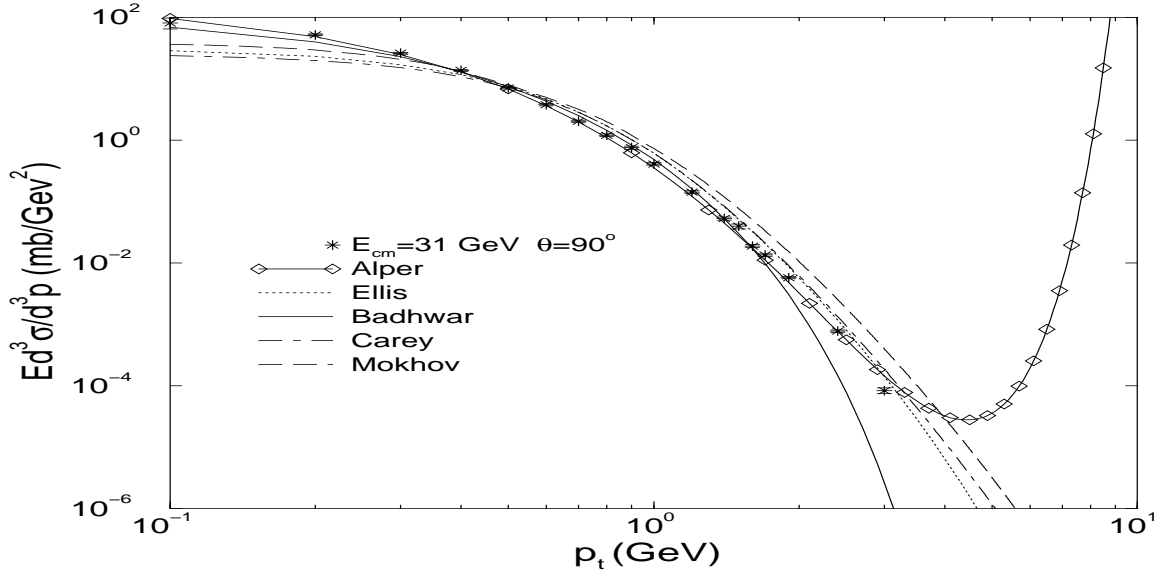


Figure 8:  $\pi^-$  production. Same as Figure 7 except  $E_{cm} = 31$  GeV, and the parametrization of Alper *et al.* (equation 13) [25] is included.

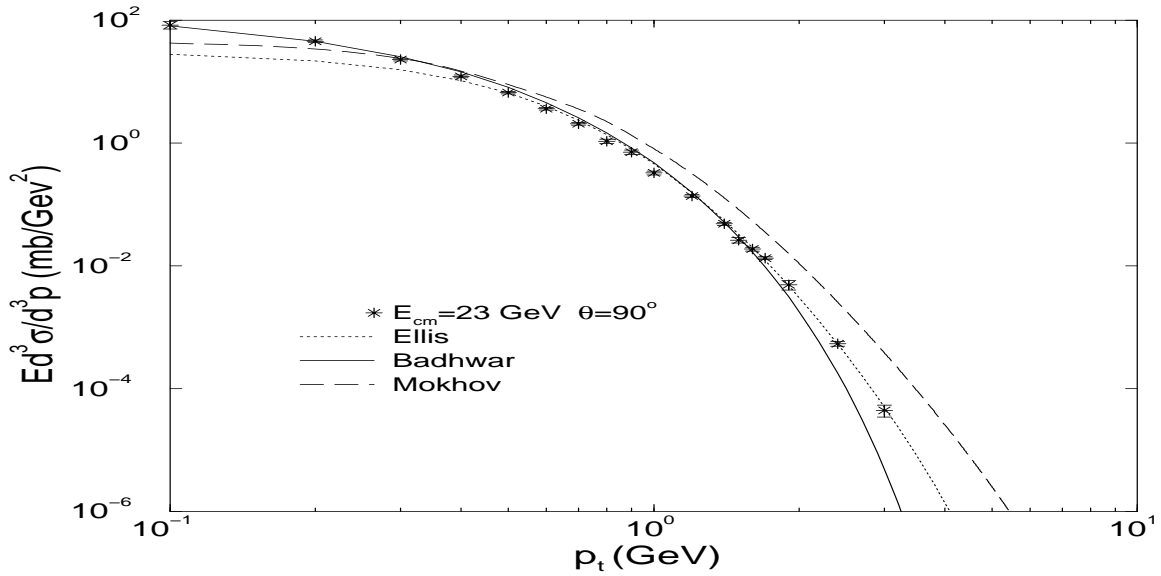


Figure 9:  $\pi^+$  production parametrizations of Ellis *et al.* (equation 15) [22], Badhwar *et al.* (equation 16) [31] and of Mokhov *et al.* (equation 17) [32] plotted with LIDCS data from [25]. LIDCS is plotted against transverse momentum for COM energy  $E_{cm} = 23$  GeV and pion COM scattering angle  $\theta^* = 90^\circ$

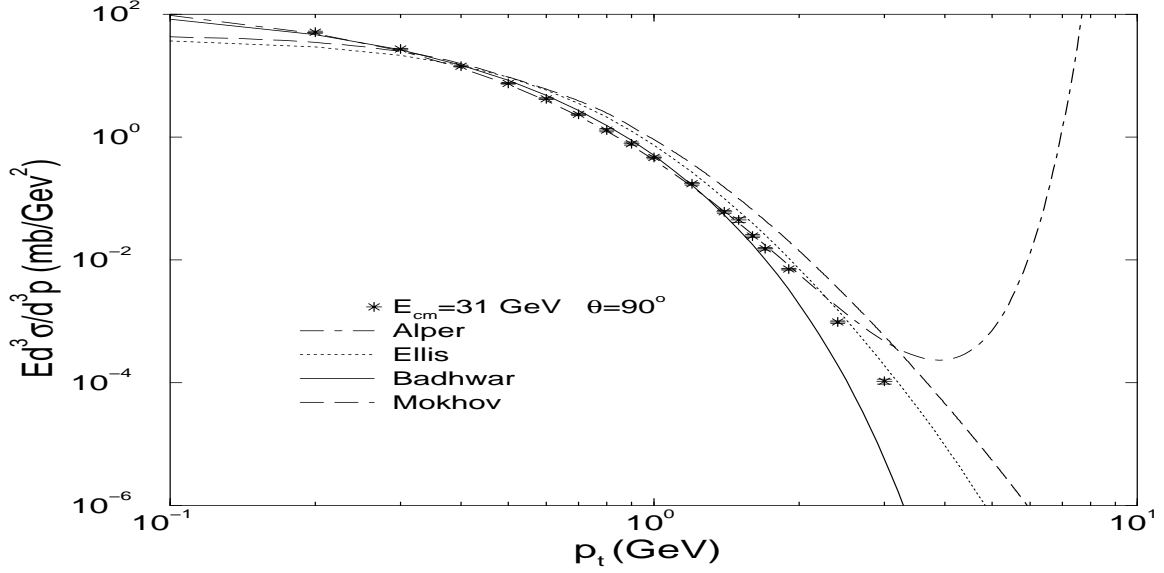


Figure 10:  $\pi^+$  production. Same as Figure 9 except  $E_{cm} = 31$  GeV, and the parametrization of Alper *et al.* (equation 13) [25] is included.

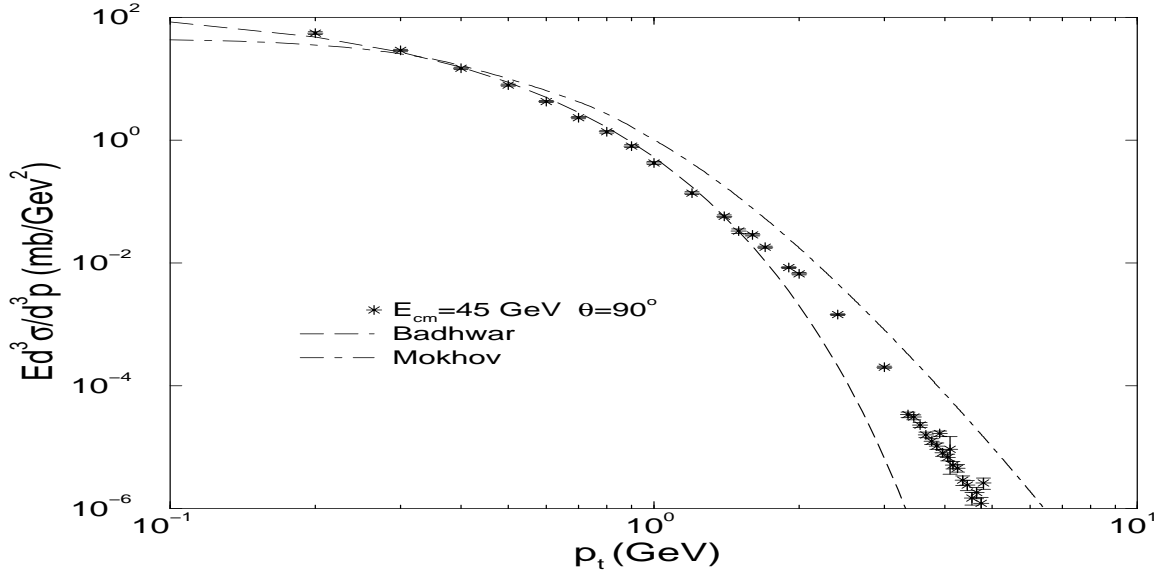


Figure 11:  $\pi^+$  production. Same as Figure 9 except the data is from [16, 25] for  $E_{cm} = 45.0$  GeV and 44.8 GeV, and the parametrization of Ellis *et al.* (equation 15) [22] is excluded. Parametrizations are plotted at  $E_{cm} = 45.0$  GeV.

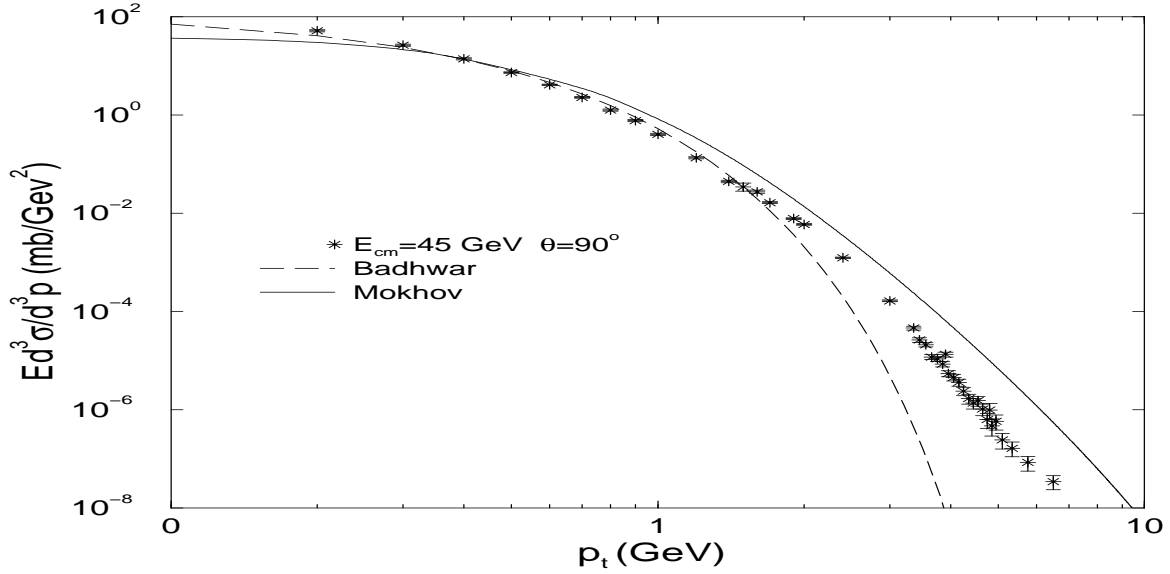


Figure 12:  $\pi^-$  production. Same as Figure 7 except the data is from [16, 25] for  $E_{cm} = 45.0$  GeV and 44.8 GeV, and some of the parametrizations are excluded. Parametrizations are plotted at  $E_{cm} = 45.0$  GeV.

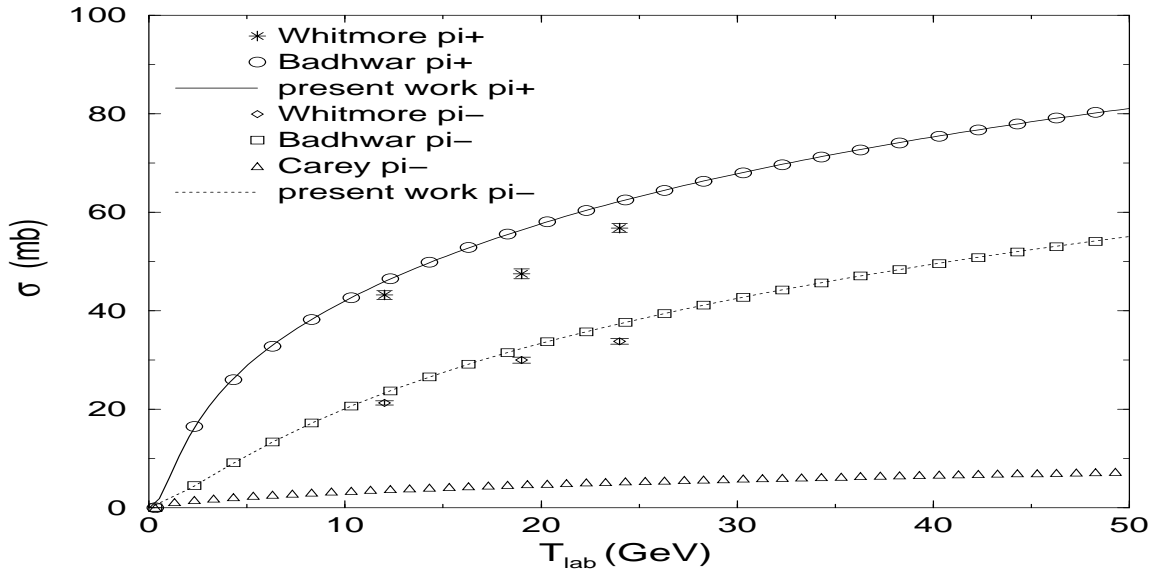


Figure 13: Parametrizations of total  $\pi^\pm$  production cross section (present work) (equations 30 and 31) plotted with numerically integrated LIDCS parametrizations of Badhwar *et al.* (equation 16) [31] (circles and squares) and Carey *et al.* (equation 14) [30] (triangles). Six data points are included for comparison (data is from Whitmore [24]).

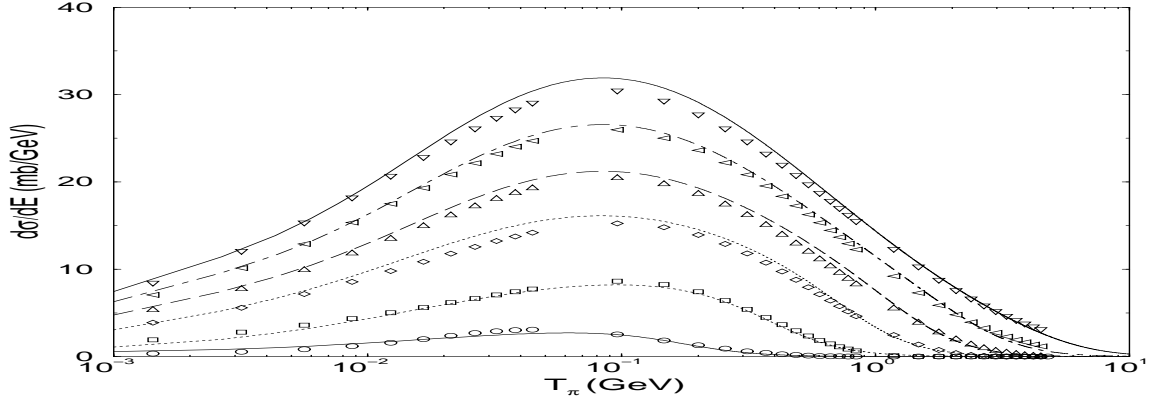


Figure 14:  $\pi^-$  spectral distribution parametrizations (equations 27 and 28) (solid lines) plotted with LIDCS parametrization of Badhwar *et al.* (equation 16) [31] (symbols) numerically integrated at lab kinetic energies of 0.5 GeV, 1.9 GeV, 5.0 GeV, 9.5 GeV, 20 GeV, and 50 GeV, listed in order of increasing cross section.

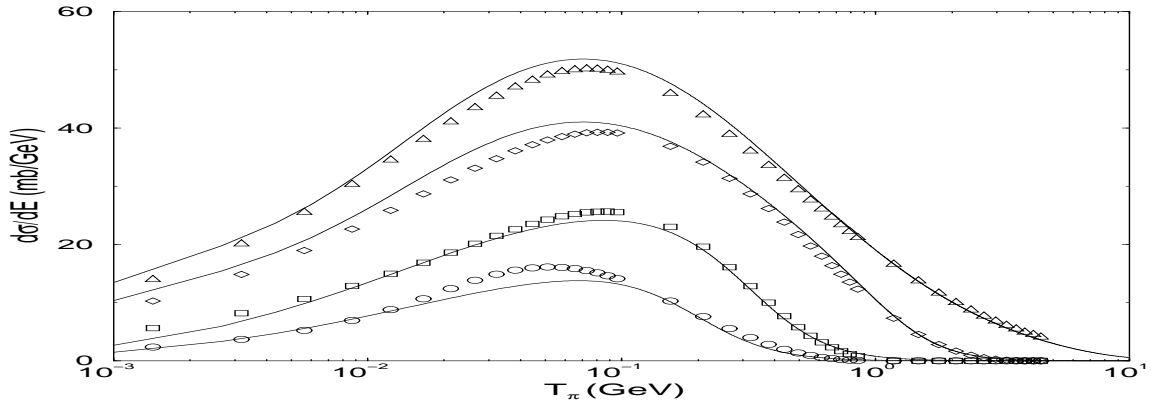


Figure 15:  $\pi^+$  spectral distribution parametrizations (equations 25 and 26) (solid lines) plotted with LIDCS parametrization of Badhwar *et al.* (equation 16) [31] (symbols) numerically integrated at lab kinetic energies of 0.5 GeV, 1.1 GeV, 5.0 GeV, and 50 GeV, listed in order of increasing cross section.